Draft, April 26, 2003

Basic mechanisms of the beam diffusion and the luminosity lifetime

V. Lebedev

Content

1. Particle scattering and absorption on the residual gas and in the IP
2. Intrabeam scattering
3. Intensity loss and bunch lengthening due to longitudinal diffusion
4. Parametric model of the collider luminosity development
5. Effects of beam-beam interaction and non-linearity of the lattice on particle diffusion
6. Luminosity scenario for final Run II parameters

1. Parametric model of the collider luminosity development

Numerous effects and beam parameters affect the Tevatron collider luminosity. Each store is different and because of finite instrumentation resolution and accuracy it is practically impossible to state what was different or what came wrong for every particular store. Nevertheless the luminosity development is very similar for most of the stores. It is driven by some basic processes, which are not very sensitive to the details of distribution functions, and therefore the luminosity evolution can be described by comparatively simple parametric model developed in the following sections. The model takes into account the major beam heating and particle loss mechanisms. They are (1) the emittance growth and the particle loss due to scattering on the residual gas, (2) the particle loss and the emittance growth due to scattering in IPs, (3) the transverse and longitudinal emittance growth due to intrabeam scattering, (4) the bunch lengthening due to RF noise, and (5) the particle loss from the bucket due to heating of longitudinal degree of freedom. If the collider tunes are correctly chosen, the beam intensity is not very high, and the beams are well formed then the beam-beam effects are not very important and the model comparatively well describes the observed dynamics of beam parameters and the luminosity. Section 5 discusses how the beam-beam effects and lattice non-linearities can be incorporated into the model and some preliminary results. The developed model is applied to the luminosity evolution for the final Run II parameters in Section 6.

1.1. Particle scattering and absorption on the residual gas and in IP

If aperture limitations are sufficiently large in comparison with the beam size ($A_{x,y} \geq 5\sigma_{x,y}$), then the multiple and single scattering on the residual gas atoms can be considered separately. In this case the single scattering causes thee particle loss, while the multiple scattering causes the emittance growth.

The beam lifetime due to single scattering is described by the well-known formula

$$t_{scat}^{-1} = = \frac{2pcr_p^2}{g^2 b^3}\left(\sum_i Z_i(Z_i+1)\left(\frac{\overline{b_x n_i}}{e_{mx}} + \frac{\overline{b_y n_i}}{e_{my}}\right)\right) + \sum_i n_i s_i c b \quad , \qquad (1)$$

where $\overline{b_{x,y} n_i} = \int b_{x,y} n_i ds \Big/ C$ are the average gas density weighted by beta-functions, $e_{mx,my}$ are the horizontal and vertical acceptances, r_p is the proton classical radius, g and b are the relativistic factors, summing is performed over all residual gas species, and averaging is performed over ring circumference. The first addend is related to the electromagnetic scattering and the second to the strong interaction. Taking into account that the scattering angle due to strong interactions ($q \sim m_\pi/p \approx 140$ μrad) significantly exceeds rms angles in the beam (~7 μrad) s_i can be considered to be the total nuclear cross section with sufficiently good accuracy. The beam based measurements of the average residual gas pressure[1] yield that the average pressure in the ring is about 10^{-9} Torr of molecular nitrogen equivalent. It is also verified by the results of the luminosity parametric model presented below. At the collision energy of 980 GeV the beam lifetime is dominated by the strong interaction.

The emittance growth rate due to multiple scattering is closely related to the

electromagnetic part of the single scattering lifetime and is determined by the following formula[1]

$$\frac{de_{x,y}}{dt} = \frac{2pcr_p^{\,2}}{g^2 b^3}\left(\sum_i \overline{b_{x,y} n_i} Z_i (Z_i + 1) L_c\right) \quad , \tag{2}$$

where L_c is the Coulomb logarithm ($L_c \approx 9$). Tables 1 and 2 present parameters used in the simulations. As far as we can judge now these parameters represent present vacuum conditions in Tevatron and we do not expect significant vacuum improvements in the future.

Table 1. Gas composition used in the simulations

Gas	H_2	CO	N_2	C_2H_2	CH_4	CO_2	Ar
Pressure [nTorr]	5.7	0.14	0.07	0.06	0.11	0.07	0.09

Table 2. Model parameters used in the simulations

Effective N_2 equivalent pressure, $\sum Z_i (Z_i + 1) n_i / (2 \cdot 7 \cdot 8)$	$1.01 \cdot 10^{-9}$ Torr
Average ring beta-functions, b_x/b_y	71.5 m/71.7 m
Normalized acceptance	720 mm mrad
Electromagnetic scattering lifetime	15,000 hour
Nuclear scattering/absorption lifetime	306 hour
Total single scattering lifetime	300 hour
Normalized 95% emittance growth rate, $6g de_{x,y}/dt$	0.17 mm mrad/hour

Similar to the gas scattering the scattering in the interaction point (IP) can be separated into the single scattering due to strong interaction and the emittance growth due to electromagnetic scattering. The total $\bar{p}p$ cross section consists of two parts: the inelastic cross section of 60 mbarn and the elastic cross section of 15 mbarn at 1 TeV energy. All particles scattered inelastically are lost immediately, while as shown in Ref. 2 about 40% of elastically scattered particles remain in the beam (within 3σ). That is related to the small beta-function in IP and, consequently, large particle angles so that the scattering angles are comparable to the particle angles (~100 μrad). Summing effects of elastic and inelastic interactions we obtain the total cross section of particle loss equal to 69 mbarn.

The emittance growth due to electromagnetic scattering equal to

$$\frac{de_{x,y}}{dt} = \frac{4r_p^{\,2} N L_{bb} f_0}{g^2 b^3 \sqrt{(e_{px} + e_{py})(e_{ax} + e_{ay})}} \tag{3}$$

for one IP. Here e_{px}, e_{py}, e_{ax} and e_{ay} are the emittances for proton and antiproton beams, f_0 is the revolution frequency, L_{bb} is the Coulomb logarithm ($L_{bb} \approx 20$), and N is the number of particles in the counter-rotating bunch. For two IPs and present Tevatron parameters it yields the antiproton emittance growth rate of about 0.01 mm mrad/hour. Although emittance growth rate is almost negligible in comparison with gas scattering the nuclear absorption in the IP is the main mechanism for antiproton loss during collisions.

[1] We use the non-normalized rms emittances, e_x, e_y, in all formulas throughout this document; but all numerical values are quoted for the standard Fermilab emittance definition - the 95% normalized emittances, e_{nx}, e_{ny},. Two definitions are bound up by the following formula $e_{nx,ny} = 6g e_{x,y}$.

1.2. Intrabeam scattering

Another important diffusion mechanism is determined by intrabeam scattering (IBS). For the Tevatron collider parameters the longitudinal energy spread in the beam frame is significantly smaller than the transverse ones ($v_\parallel/v_\perp \approx 0.02$ at collision energy, and $v_\parallel/v_\perp \approx 0.15$ at injection energy). In this case comparatively simple IBS formulas can be used. Following reference [3] we can write the following expressions for the longitudinal and transverse emittance growth rates[2]

$$\frac{d\left(\sigma_{\Delta p/p}^{\,2}\right)}{dt} = \frac{r_p^{\,2} c N}{4\sqrt{2}\gamma^3 b^3 \sigma_s} \left\langle \frac{\Xi_\parallel(q_x, q_y)}{\sqrt{q_x^{\,2}+q_y^{\,2}}} \frac{L_C}{\sigma_x \sigma_y} \right\rangle_s , \tag{4}$$

$$\frac{d\varepsilon_{x,y}}{dt} = \frac{r_p^{\,2} c N}{8\sqrt{2}\gamma^3 b^3 \sigma_s} \left\langle \frac{L_C}{\sigma_x \sigma_y \sqrt{q_x^{\,2}+q_y^{\,2}}} \begin{bmatrix} 2A_x \Xi_\parallel(q_x, q_y) - \dfrac{b_x}{\gamma^2} \Xi_\perp(q_x, q_y) \\ -\dfrac{b_y}{\gamma^2} \Xi_\perp(q_y, q_x) \end{bmatrix} \right\rangle_s . \tag{5}$$

Here $\sigma_{\Delta p/p} \equiv \sqrt{\overline{(p_\parallel/p)^2}}$ is the rms momentum spread, σ_s is the rms bunch length,

$$\sigma_x = \sqrt{\varepsilon_x \beta_y + D_x^{\,2} \sigma_\parallel^{\,2}}, \qquad \sigma_y = \sqrt{\varepsilon_y \beta_y},$$
$$q_x = \sqrt{\frac{\varepsilon_x}{\beta_x}\left(1 + \frac{\left(D_x' \beta_x + \alpha_x D_x\right)^2 \sigma_{\Delta p/p}^{\,2}}{\varepsilon_x \beta_x + D_x^{\,2} \sigma_{\Delta p/p}^{\,2}}\right)}, \qquad q_y = \sqrt{\varepsilon_y/\beta_y} \tag{6}$$

are the rms sizes and local angular spreads along the ring, β_x, β_y, α_x and α_y, are beta- and alpha-functions, D_x and D_x' are the dispersion and its derivative, $\langle\ \rangle_s$ denotes averaging over the ring,

$$A_x = \frac{D_x^{\,2} + \left(D_x' \beta_x + \alpha_x D_x\right)^2}{\beta_x} \tag{7}$$

is the horizontal motion invariant, and

$$L_C = \ln\left(\frac{r_{\max}}{r_{\min}}\right), \quad r_{\max} = \min\left(\sigma_x, \sigma_y, \sqrt{\frac{q_x^{\,2}+q_y^{\,2}}{N r_p}\gamma^3 b^2 \sigma_x \sigma_y \sigma_s}\right), \quad r_{\min} = \frac{2 r_p}{\gamma^2 b^2 \left(q_x^{\,2}+q_y^{\,2}\right)} \tag{8}$$

is the Coulomb logarithm ($L_C \approx 23$). Functions

$$\Xi_\parallel(x, y) \approx 1 + \frac{\sqrt{2}}{p} \ln\left(\frac{x^2+y^2}{2xy}\right) - 0.055\left(\frac{x^2-y^2}{x^2+y^2}\right)^2, \tag{9}$$

$$\Xi_\perp(x, y) \approx 1 + \frac{2\sqrt{2}}{p} \ln\left(\frac{\sqrt{3x^2+y^2}}{2y^2}\, x\right) + \frac{0.5429 \ln(y/x)}{\sqrt{1+\ln^2(y/x)}} \tag{10}$$

---

[2] A comparison of these equations with the Bjorken-Mtingwa formulas[4] for the case $v_\parallel << v_\perp$ exhibited their identity when exact integral presentations are used for functions $\Xi_\parallel(x, y)$ and $\Xi_\perp(x, y)$. In the case of their approximate representation considered here the results coincide within a few percent.

approximate exact results (obtained for Gaussian distribution for all three degrees of freedom) with accuracy better than a few percent. That is sufficiently good for all practical applications. The energy conservation requires $\Xi_{\perp}(x,y)+\Xi_{\perp}(y,x)=2\Xi_{\parallel}(x,y)$, which is fulfilled with better than 1% accuracy.

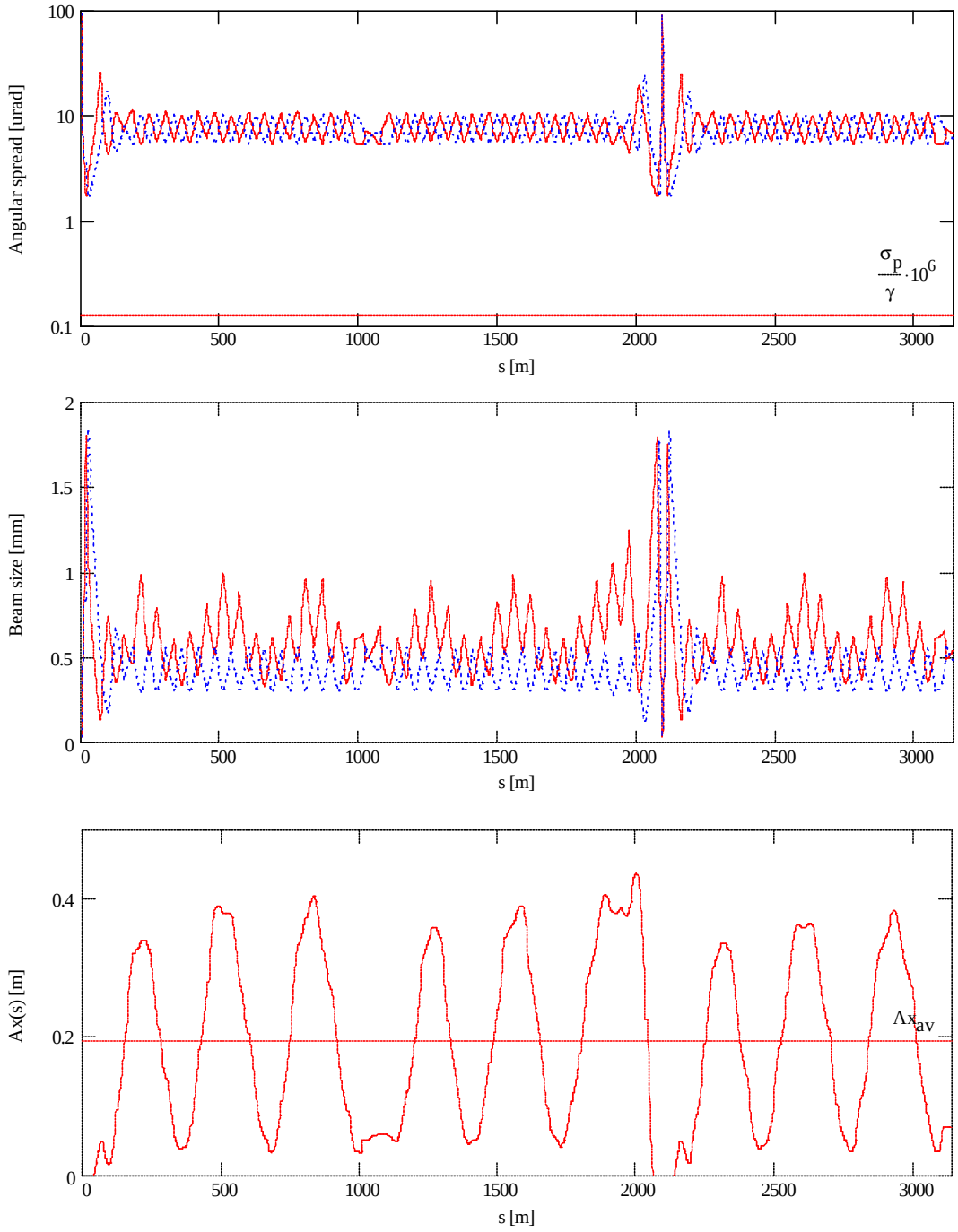

Figure 1. Rms angular spreads (top), rms beam sizes (center) and the horizontal motion invariant A_x (bottom) and for half Tevatron circumference (from B0 to E0); solid lines – horizontal degree of freedom, dashed lines – vertical degree of freedom. Transverse normalized 95% beam emittances are 19 mm mrad, longitudinal energy spread is $1.35\cdot10^{-4}$. Horizontal line on the top plot shows longitudinal "angle" in the beam frame.

Tevatron has sufficiently smooth lattice and therefore IBS can be described with good accuracy in the smooth approximation. In this case Eq. (4) and (5) can be rewritten as following

$$\begin{bmatrix} ds_{\Delta p/p}{}^2/dt \\ de_x/dt \\ de_y/dt \end{bmatrix} = \frac{r_p{}^2 cNL_C \Xi_{\|}(\bar{q}_x, \bar{q}_y)}{4\sqrt{2}g^3 b^3 \bar{s}_x \bar{s}_y s_s \sqrt{\bar{q}_x{}^2 + \bar{q}_y{}^2}} \begin{bmatrix} 1 \\ \bar{A}_x(1-k) \\ \bar{A}_x k \end{bmatrix} \quad , \tag{11}$$

where

$$\bar{s}_x = \sqrt{e_x \bar{b}_y + \bar{D}_x{}^2 s_{\Delta p/p}{}^2}, \qquad \bar{s}_y = \sqrt{e_y \bar{b}_y},$$
$$\bar{q}_x = \sqrt{e_x/\bar{b}_x}, \qquad \bar{q}_y = \sqrt{e_y/\bar{b}_y}. \tag{12}$$

For Tevatron the averaged beta-functions, dispersion and the horizontal motion invariant are $\bar{b}_x = R/n_x =$ 49 m, $\bar{b}_y = R/n_y =$ 49 m, $\bar{D}_x = \int D_x ds/2pR =$2.84 m, and $\bar{A}_x = \int A_x ds/2pR =$0.2 m. To get Eq. (11) we neglected in Eq. (5) the addends with $\Xi_{\perp}(x, y)$ which make only small correction but we introduced the coupling parameter k which takes into account the redistribution of heating between horizontal and vertical degrees of freedom. Presently we do not know our optics with sufficient accuracy so that we could independently calculate k. Experimental value is about 0.3, and it is used in the model.

Figure 1 presents beam sizes and angular spreads for half Tevatron at collisions. One can see that the longitudinal velocity spread is much smaller than the transverse one through the entire ring. That validates the use of simplified IBS formulas of Eqs. (4) and (5). Averaging these equations over the ring for beam parameters of Figure 1, the rms bunch length of 62 cm, zero coupling (k = 0) and $1.6 \cdot 10^{11}$ protons/bunch yields the horizontal and longitudinal emittance growth lifetimes of 22.5 and 28.5 hours, correspondingly. The use of smooth approximation formulas of Eq. (11) yields 18.9 and 26.9 hours. As one can see the difference is sufficiently small and therefore the smooth approximation has been used in the described below parametric model.

1.3. Intensity loss and bunch lengthening due to diffusion

The length of the bunch in Tevatron is large and therefore a longitudinal diffusion causes particle loss from the bucket. The diffusion equation in a sinusoidal longitudinal potential can be written in the following form

$$\frac{\partial f}{\partial t} = \frac{\partial}{\partial I}\left(\frac{\tilde{D}(I)}{dE/dI} \frac{\partial f}{\partial I} \right), \tag{13}$$

where the action and the energy are

$$I = \frac{1}{2p} \oint p df \quad , \quad E = \frac{p^2}{2} + \Omega_s{}^2 (1 - \cos f) \quad . \tag{14}$$

The solution of Eq. (13) was performed numerically for the case of constant diffusion, and zero length bunch $f(I) = d(I)$. The boundary condition $f(I)$ = 0 at the RF bucket boundary is used. It is justified by the fact that only small fraction (36/1113) of the buckets are filled. Particles, which leave the bucket, become smoothly distributed through

the entire ring. That immediately drops particle density by almost 2 orders of magnitude. Additionally, particles are decelerated by synchrotron radiation and leave the ring in about 20 minutes after they left the bucket.

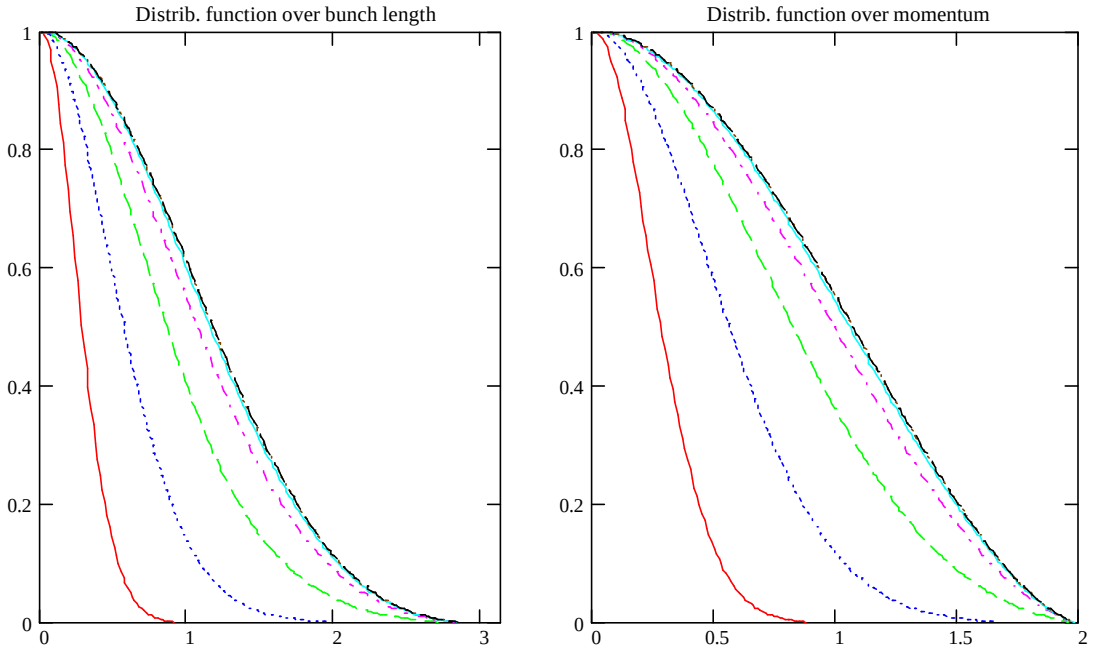

Figure 2. Dependence of distribution functions over bunch length and momentum on time obtained by numerical solving Eq. (13) for constant diffusion. Curves show the distribution sequentially for the following times: DT = 0.0625, 0.25, 0.562, 1.0, 1.56, 2.25, 3.06.

Resulting distribution functions over bunch length and momentum are presented in Figure 2. Figure 3 presents time dependence of rms bunch length and momentum on time, and Figure 4 presents relative bunch intensity on time. As one can see, initially, while the whole bunch is located in the linear part of potential well the rms bunch length and momentum spread are equal and grow proportionally to $\sqrt{Dt}$. Then, when the potential well shallows, the bunch length grows faster than the momentum spread and, finally, both of them come to their asymptotic values: $s_f \approx 0.930$ rad and $s_p \approx 0.765$. At that time the intensity dependence on time and distribution functions also come to its asymptotic behaviors. The intensity decays exponentially, $I \propto \exp(-1.35Dt)$.
As one can see from Figure 2 the asymptotic distribution function over bunch length is sufficiently close to the Gaussian, but the asymptotic distribution function over momentum is almost parabolic.

The results of simulations yield the following approximate relationships between the bunch parameters

$$s_s \approx \Gamma_s s_{\Delta p/p}\left(1+\frac{1}{4}\left(\frac{2s_{\Delta p/p}}{\Delta P/P\big|_{sep}}\right)^2+\frac{1}{6}\left(\frac{2s_{\Delta p/p}}{\Delta P/P\big|_{sep}}\right)^3\right) , \qquad (15)$$

$$\frac{1}{N}\frac{dN}{dt}\bigg|_L \approx \frac{2.425\,(2p s_s)^7}{l_{RF}{}^7+1.65\,(2p s_s)^7}\left(\left(\frac{2p\Gamma_s}{l_{RF}}\right)^2\frac{d\left(s_{\Delta p/p}{}^2\right)}{dt}\bigg|_{IBS}+\frac{d\left(s_f{}^2\right)}{dt}\bigg|_{RF}\right) , \qquad (16)$$

$$\left.\frac{d\left(s_{\Delta p/p}^{\,2}\right)}{dt}\right|_{total} \approx \left(1-\left(\frac{2s_{\Delta p/p}}{0.765\Delta P/P\big|_{sep}}\right)^5\right)\left(\left.\frac{d\left(s_{\Delta p/p}^{\,2}\right)}{dt}\right|_{IBS}+\left(\frac{l_{RF}}{2p\Gamma_s}\right)^2\left.\frac{d\left(s_f^{\,2}\right)}{dt}\right|_{RF}\right), \qquad (17)$$

where $\Gamma_s = \left(a - 1/g^2\right) q\, l_{RF} / (2p n_s)$ is the parameter of longitudinal focusing, l_{RF} is the wave length of the RF voltage, n_s it the longitudinal tune, a is the momentum compaction, q is the harmonic number and $\Delta P/P\big|_{sep}$ is the height of the RF bucket. There are two addends in Eqs. (16) and (17). The first addend is related to the momentum growth due to IBS and is determined by Eq. (11) in the parametric model described below. The second addend is related to the emittance growth due to RF noise with the growth rate for small amplitude equal to

$$\left.\frac{d\left(s_f^{\,2}\right)}{dt}\right|_{RF} = p\,\Omega_s^{\,2}\left(P_f(\Omega_s)+\frac{1}{2}s_f^{\,2}P_A(2\Omega_s)\right) \quad . \qquad (18)$$

Here s_f is the bunch length in radians, Ω_s is the synchrotron frequency, and the spectral densities of the phase and amplitude noise are normalized as following

$$\overline{df_{RF}^{\,2}} = \int_{-\infty}^{\infty} P_f(w)dw \quad , \quad \frac{\overline{dA_{RF}^{\,2}}}{A_{RF}^{\,2}} = \int_{-\infty}^{\infty} P_A(w)dw \quad . \qquad (19)$$

The affect of the RF noise on the beam is dominated by the RF phase noise[3]. Presently its spectral density[5] is about $P_{ff}(\Omega_s/2p) = 4pP_f(\Omega_s) \approx 6\cdot 10^{-12}$ rad^2/Hz, which causes the bunch lengthening of about 16 mrad/hour$^{1/2}$. This value is almost two orders of magnitude smaller than the longitudinal emittance growth due to IBS at the nominal proton intensity.

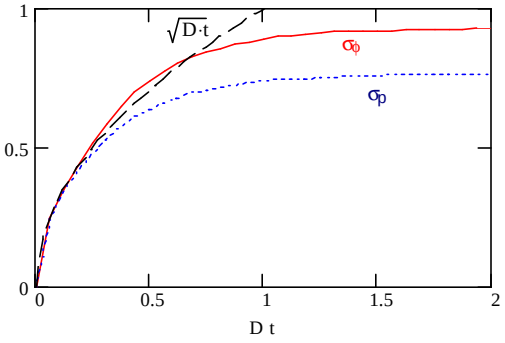

Figure 3. Dependence of rms bunch length (solid line) and momentum spread (dotted line) on time. Bunch length is expressed in radians. Momentum spread is expressed in $2p/p_{max}$ units, where p_{max} in the size of the bucket. Dashed line presents the dependence of bunch length and momentum spread on time for linear oscillator.

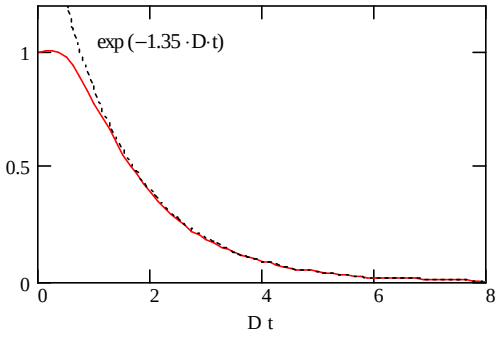

Figure 4. Dependence of relative bunch intensity (solid line) on time. Dotted line shows asymptotic exponential decay of the beam intensity.

[3] Main source of RF phase noise is a microphonics exited in a cavity due to flow of cooling water. RF phase feedback suppresses the noise by 30 db. That brings the noise to an acceptable level.

1.4. Parametric model

For gaussian beams the luminosity of the collider is determined by the well-known formula:

$$L = \frac{f_0 n_b N_p N_a}{2\pi b^* \sqrt{(e_{px}+e_{ax})(e_{py}+e_{ay})}} H\left(\frac{\sqrt{s_{sp}^2 + s_{sp}^2}}{\sqrt{2}b^*}\right) , \qquad (20)$$

where n_b is the number of bunches, N_p and N_a are the number of protons and antiprotons per bunch, b^* is the beta-function in the interaction point (IP) and e_{px}, e_{py}, e_{ax} are e_{ay} are the horizontal and vertical emittances for proton and antiproton beams. The hourglass factor $H(x)$ takes into account final value of the longitudinal bunch size. It is equal to

$$H(x) = \frac{2}{\sqrt{\pi}} \int_0^\infty \frac{e^{-y^2}}{1+x^2 y^2} dy \xrightarrow{x \le 3} \approx \frac{1}{\sqrt[3]{1+1.3x^2}} . \qquad (21)$$

To describe the evolution of the luminosity we write a system of differential equations, which bounds up all basic parameters of the proton and antiproton beams:

$$\frac{d}{dt}\begin{bmatrix} e_{px} \\ e_{py} \\ s_{pp}^2 \\ N_p \\ e_{ax} \\ e_{ay} \\ s_{pa}^2 \\ N_a \end{bmatrix} = \begin{bmatrix} 2de_{px}/dt\big|_{BB} + de_{px}/dt\big|_{IBS} + de_{px}/dt\big|_{gas} \\ 2de_{py}/dt\big|_{BB} + de_{py}/dt\big|_{IBS} + de_{py}/dt\big|_{gas} \\ ds_{pp}^2/dt\big|_{total} \\ -N_p t_{scat}^{-1} - dN_p/dt\big|_L - 2Ls_{p\bar{p}}/n_b \\ 2de_{ax}/dt\big|_{BB} + de_{ax}/dt\big|_{IBS} + de_{ax}/dt\big|_{gas} \\ 2de_{ay}/dt\big|_{BB} + de_{ay}/dt\big|_{IBS} + de_{ay}/dt\big|_{gas} \\ ds_{pa}^2/dt\big|_{total} \\ -N_a t_{scat}^{-1} - dN_a/dt\big|_L - 2Ls_{p\bar{p}}/n_b \end{bmatrix} . \qquad (22)$$

Here indices p and a denote protons and antiprotons, the derivatives $de/dt\big|_{BB}$ are the emittance growth rates due to scattering in the IP determined by Eq. (3) (factor of 2 takes into account 2 IPs), the derivatives $de/dt\big|_{IBS}$ are the emittance growth rates due to IBS determined by Eq. (11), the derivatives $de/dt\big|_{gas}$ are the emittance growth rates due to multiple scattering on the residual gas determined by Eq. (1), the derivatives $ds^2/dt\big|_{total}$ are the momentum spread growth rates determined by Eq. (17), the derivatives $dN/dt\big|_L$ are the particle loss rate from bucket determined by Eq.(16), and the addends $2Ls_{p\bar{p}}/n_b$ determines particle loss in two collision points due to luminosity.

Figure 5 presents measured and computed bunch parameters for the Store 2138 (Jan.05.2003), which is comparatively well described by the model. The only free parameters used in the model were the residual gas pressure of $2 \cdot 10^{-10}$ Torr of molecular nitrogen equivalent, the coupling parameter k = 0.45, and the spectral density of RF phase noise of $2.4 \cdot 10^{-11}$ rad^2/Hz. They correspond to the beam lifetime t_{gas} = 1300 hour, and the bunch lengthening $\sqrt{ds_f^2/dt\big|_{RF}}$ = 33 mrad/√hour. These values are also in a good agreement with other measurements.

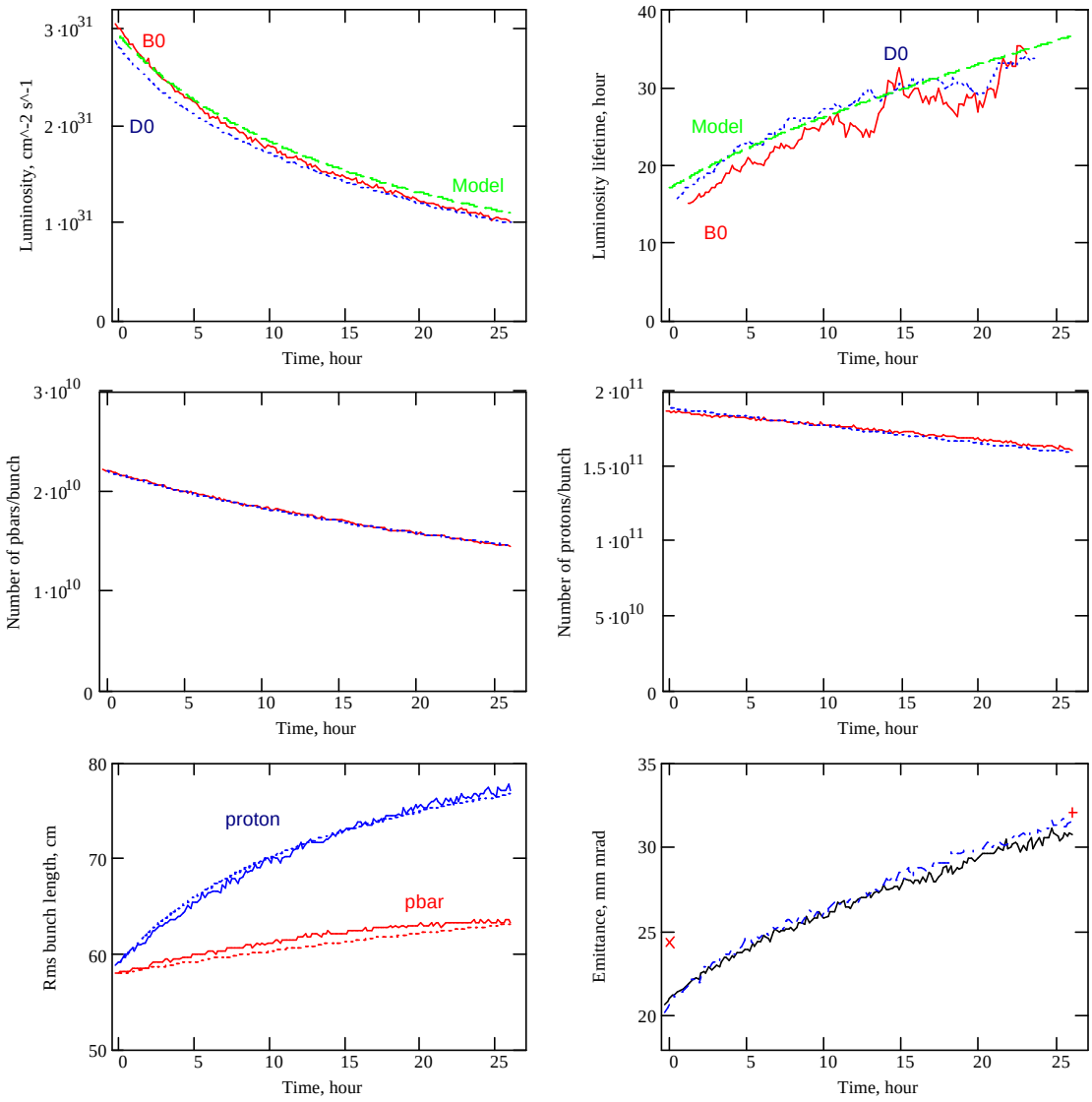

Figure 5. Dependencies of the luminosity and luminosity lifetime (top), antiproton and proton bunch intensities (middle), bunch lengths and effective emittance (bottom) on time for Store 2138. The top pictures present the CDF, D0 and model luminosities – solid, dotted and dashed lines correspondingly. The middle and left-bottom pictures present the measured (solid lines) and computed (dotted lines) intensities and longitudinal beam sizes. The right-bottom picture presents the beam effective emittances computed from the luminosity and from the emittances measured by the synchrotron light monitors. The crosses show the effective emittance build from emittances measured by the flying wires at the beginning and the end of the store.

As one can see the luminosity lifetime is overestimated by the model by ~10%. The computed proton and antiproton intensities are sufficiently close to the measured ones. At the beginning of the store the model predicts faster proton intensity decay than measured. It is related to the fact that the model overestimates the longitudinal loss from the RF bucket. The initial bucket size is about 4 eV·s. After acceleration it grows to about 10 eV·s and initially there is no particles between 4 and 10 eV·s. That is ignored in the model, which presumes the distribution function tails propagate to the end of the bucket. Measured and predicted particle losses are shown in Figure 6. Figure 7 shows computed

particle loss due to different mechanisms. As one can see the longitudinal loss from the RF bucket is the major mechanism for proton loss. The loss due to luminosity is the major mechanism for antiproton loss.

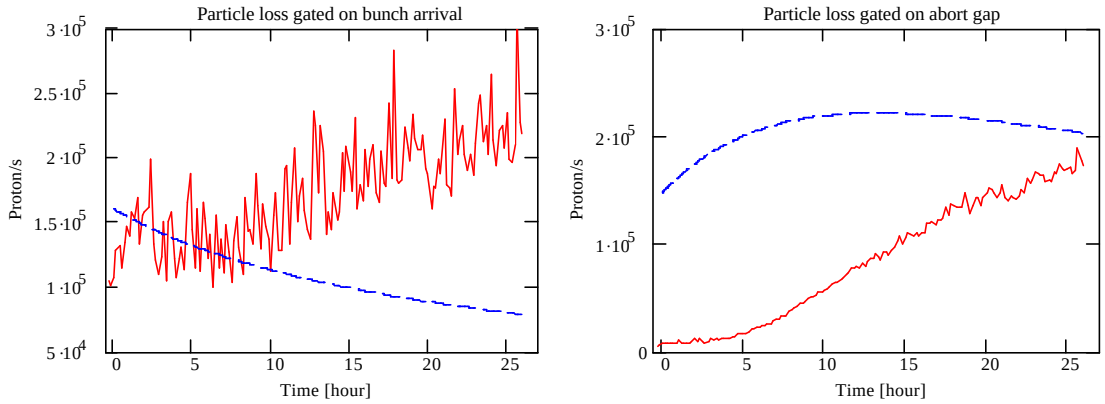

Figure 6. Dependence of computed (dashed lines) and measured particle loss per bunch on time for Store 2138.

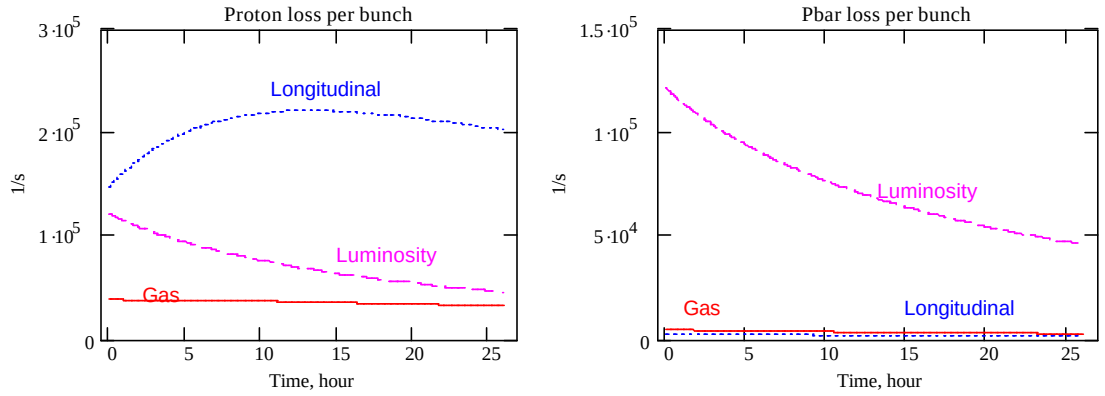

Figure 7. Dependence of particle loss on time computed from the model for different loss mechanisms for Store 2138.

The proton and antiproton lengthening (see Figure 5) is mainly driven by IBS and is in close agreement with measurement. Unfortunately there are no reliable emittance measurements and therefore some data massaging were performed to compare the measurements and the model. The right-bottom picture in Figure 5 presents the beam effective emittances,

$$e_{efff} = \sqrt{(e_{px} + e_{ax})(e_{py} + e_{ay})} \quad , \tag{23}$$

computed from the luminosity and from the emittances measured by the synchrotron light monitor. To match the curves the constant values were subtracted from the sync-light emittances. That takes out the contributions of light optics errors and diffraction. The relative scale of sync-light monitors was independently checked with local orbit bumps and found to be correct. It is also verified by coincidence of two curves in the right-bottom picture in Figure 5. Figure 8 presents comparison of the corrected sync-light emittances, the emittances measured by flying wires at the beginning and at the end of the store and model emittances which initial values were adjusted to match the luminosity, bunch lengthening, and the flying wires emittance measurements at the end of the store. One can see that both proton and antiproton vertical emittances grow significantly faster

than the model prediction. This is the major reason while measured luminosity decay time (see Figure 5) is ~10% below the model predictions. Our present belief is that it is related to amplification of the diffusion by the beam-beam effects (see next section).

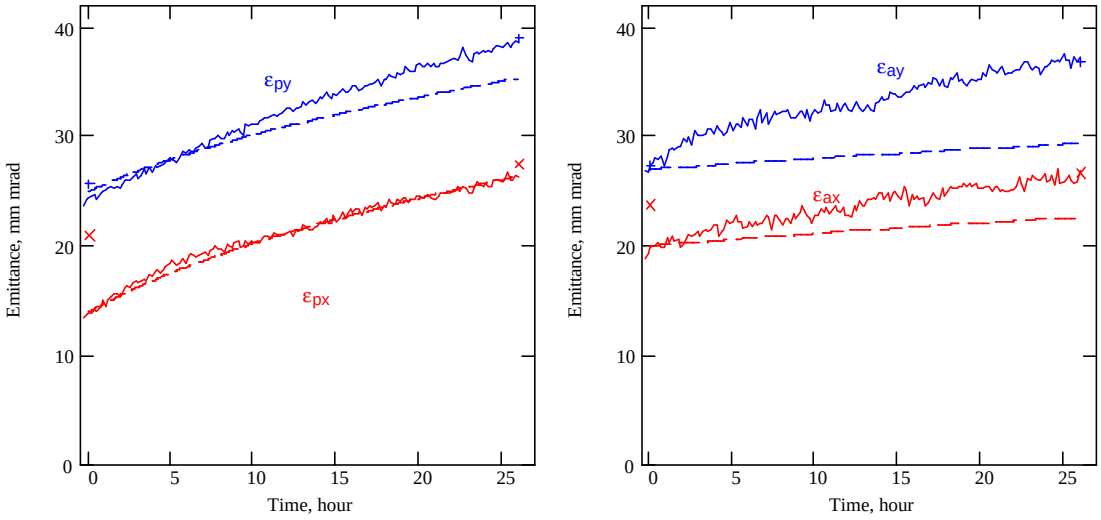

Figure 8. Dependence of proton (left) and antiproton (right) beam emittances on time for Store 2138; solid lines – the emittances measured by sync-light monitors; dashed lines – the computed emittances, crosses - the emittances measured by flying wires at the beginning and at the end of the store. The following values were subtracted from the sync-line emittances: Δe_{px}=17 mm mrad, Δe_{py}=5 mm mrad, Δe_{ax}=21 mm mrad, Δe_{ay}= 5 mm mrad.

The store 2138 discussed above has moderate discrepancies with the model and from this point of view can be considered as a normal store. The most of our stores are stronger influenced by the beam-beam interactions, but it still does not cause significant affect on the luminosity decay and the luminosity integral. Figure 9 presents measured and computed bunch parameters for the Store 2328 (Mar.20.2003). The fitting of the model to the data required an increase of vacuum from $2{\cdot}10^{-10}$ Torr for Store 2138 to $7.9{\cdot}10^{-10}$ Torr. Other free parameters were unchanged. In distinguish from Store 2138 the proton beam intensity decays faster than the model prediction, and the proton bunch length grows slower than the model prediction. Our present belief is that it is related to the beam-beam affect of antiprotons on the proton beam. The most probable reason is that small, uncontrolled changes of tunes combined with large proton bunch length affect the motion stability for particles with large synchrotron amplitudes. That causes both the particle loss and the bunch shortening (actually it was compensated by bunch lengthening due to IBS). Figure 10 demonstrates that this increase of particle loss is also well visible on the loss counters, which verify that the loss happens transversely. Figure 11 depicts computed linear tune shifts due to head-on beam-beam interactions in two IPs.

5. Luminosity scenario for final Run II parameters.

As it follows from the results presented in the previous section the beam-beam interactions certainly affect the luminosity decay, but its effect is sufficiently small and the developed parametric model, with some reservations, can be used to analyze the luminosity dynamics for the final Run II parameters. An influence of beam-beam effects and instabilities on the beam parameters and the luminosity will be discussed later.

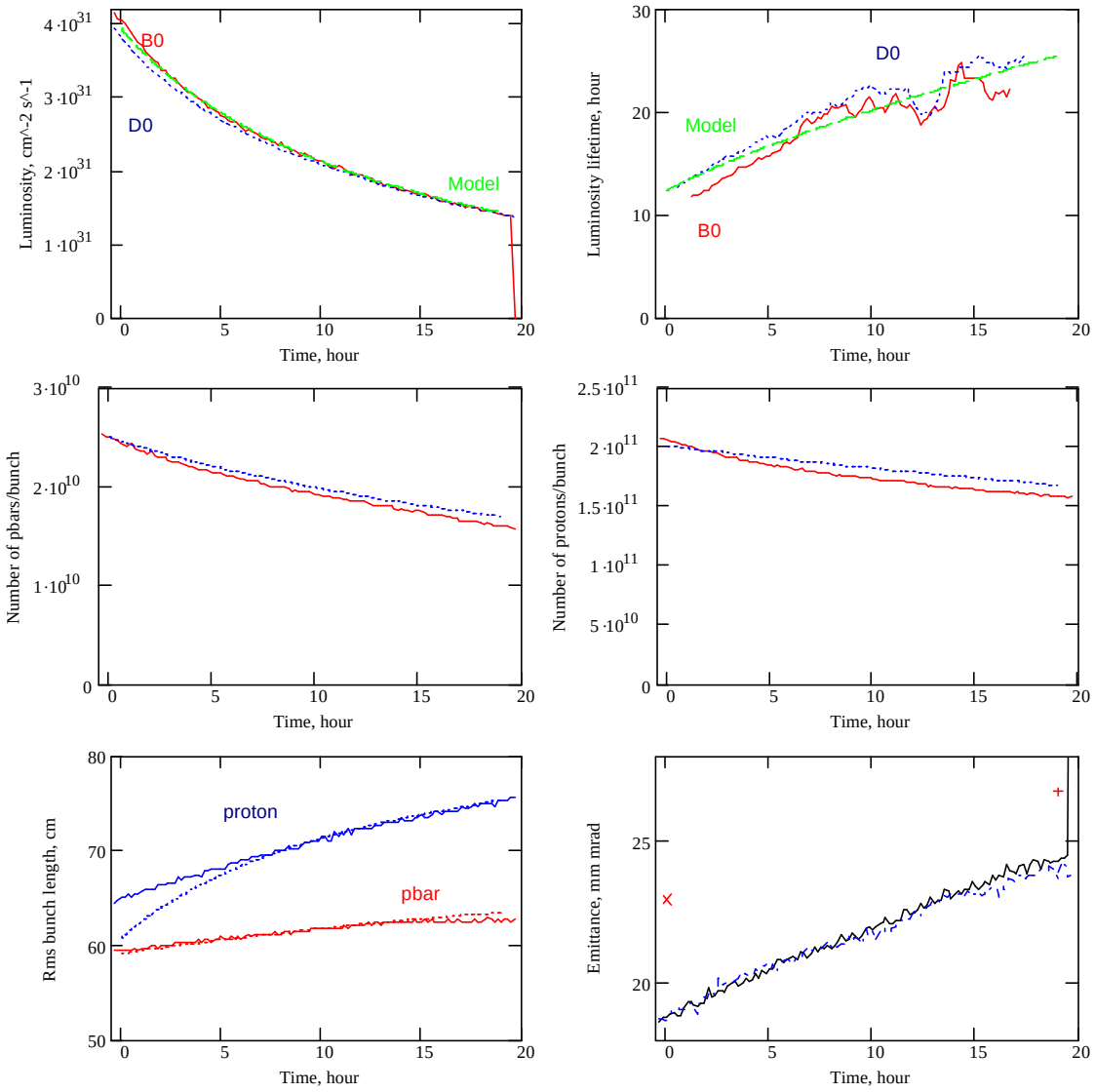

Figure 9. Dependencies of the luminosity and luminosity lifetime (top), antiproton and proton bunch intensities (middle), bunch lengths and effective emittance (bottom) on time for Store 2328. The top pictures present the CDF, D0 and model luminosities – solid, dotted and dashed lines correspondingly. The middle and left-bottom pictures present the measured (solid lines) and computed (dotted lines) intensities and longitudinal beam sizes. The right-bottom picture presents the beam effective emittances computed from the luminosity and from the emittances measured by the synchrotron light monitors. The following values were subtracted from the sync-line emittances: Δe_{px}=17 mm mrad, Δe_{py}=5 mm mrad, Δe_{ax}=14 mm mrad, Δe_{ay}= 2.5 mm mrad. The crosses show the effective emittance build from emittances measured by the flying wires at the beginning and the end of the store.

Table II presents parameters of the presently record Store 2328, typical collider parameters in April 2003 and projections for the final Run II parameters. Figure 12 depicts development of the collider parameters on time for the final Run II parameters. As one can see to achieve 7.2 times increase of the luminosity we plan to increase the number of antiprotons extracted from the stack by 4 times. The rest, 1.8 times, should come from the improvements in the antiproton transport and Tevatron. Three major contributors are an increase of the proton intensity by ~30%, an improvement of

coalescing in MI, and improvements of antiproton transport (from the antiproton stack to the collisions in Tevatron). Two last items expected to yield an increase in the transfer efficiency from ~60% to 80%. The chosen proton intensity, $2.7 \cdot 10^{11}$ per bunch, corresponds to the linear head-on tune shift of 0.01 for each of two IPs. This is the maximum tune shift achieved in Run Ib with 6×6 bunch operation. We choose the maximum antiproton intensity to be half of the proton intensity. It is expected that further increase of antiproton intensity is limited by coherent beam-beam effects (strong-strong case) and by antiproton production.

Top-left picture in Figure 12 presents the luminosity and the average luminosity computed as functions of time. The average luminosity is computed as the luminosity integral averaged over integration time and the shot setup time of 2 hour, $L_{avg}(t) = \left(t + T_{setup}\right)^{-1} \int_o^t L(t')dt'$. In distinguish from the "instant" luminosity the average luminosity achieves its peak at approximately 7 hours and after this decreases comparatively slow. That implies that if we will lose in the antiproton production rate we can compensate most of this loss by lengthening of the store time. Figure 13 presents dependence of the average luminosity on the store duration time for different antiproton production rates.

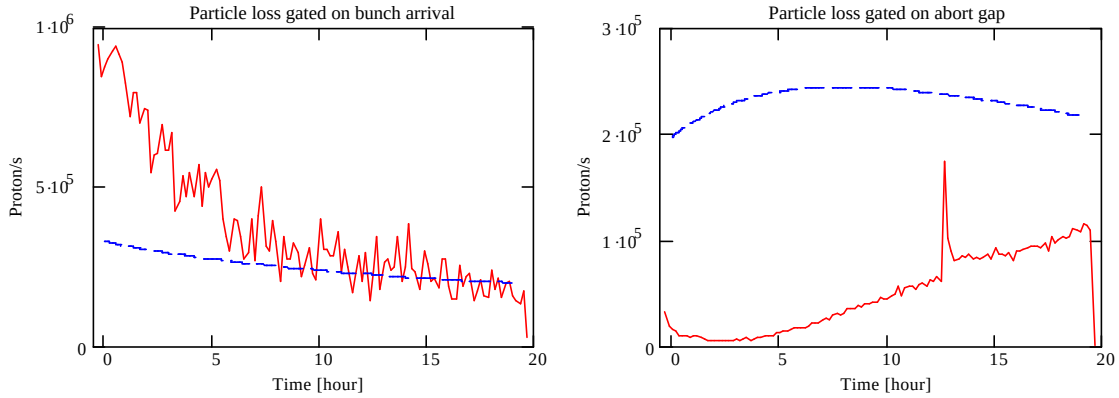

Figure 10. Dependence of computed (dashed lines) and measured particle loss per bunch on time for Store 2328.

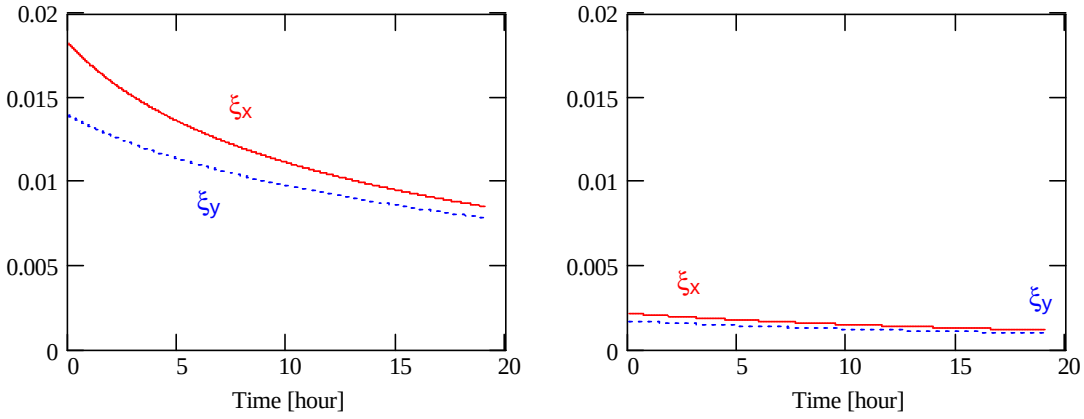

Figure 11. Dependence of computed beam-beam linear tune shifts for antiprotons (left) and protons (right) on time for Store 2328; solid lines – the horizontal tune shifts, dashed lines – the vertical tune shifts.

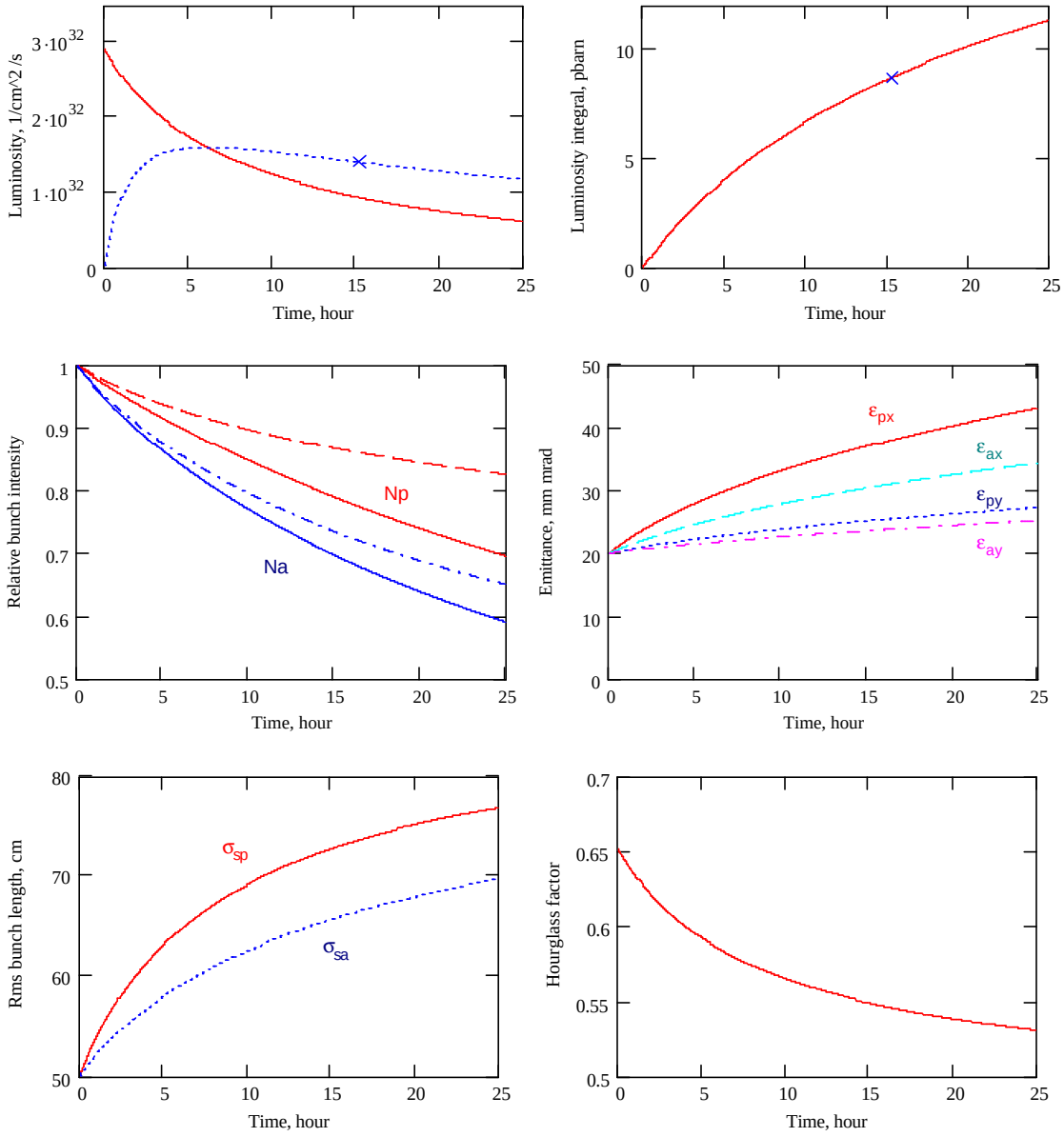

Figure 12. Dependencies on time for: *top-left* – the luminosity (solid line) and the average luminosity (dashed line); *top-right* – the luminosity integral; *middle-left* – the relative proton and antiproton intensities (solid lines) and intensity dropped due to scattering in IPs (dashed lines); *middle-right* – the beam emittances; *bottom-left* – the bunch lengths; and *bottom-right* – the hour glass factor, *H*. The crosses on the top pictures mark the store end.

Due to reduction of luminosity lifetime with growth of peak luminosity the averaged over store luminosity grows slower than the peak luminosity. The luminosity integral per year (in Table 2) is calculated presuming that the collider operates 46 weeks per year (6 weeks downtime or shutdown time); there is 48 hour downtime per week; and the shot setup time is not included into the downtime and is 2 hour.

Although IBS is the major source of beam heating there are many contributors to a finite luminosity lifetime. Table 3 presents the contributions of different beam parameter variations to the luminosity lifetime.

Table 2. Present and final Run II parameters of the collider

	Store 2328	Typical for April 2003	Final Run II
Number of protons per bunch, 10^{10}	20.7	20	27
Number of antiprotons per bunch, 10^{10}	2.54	2.2	13.5
Normalized 95% proton emittances, e_x /e_y, mm mrad	~14/24	~15/25	20/20
Normalized 95% antiproton emittances, e_x /e_y, mm mrad	~15/24	~16/25	20/20
Proton bunch length, cm	65	62	50
Antiproton bunch length, cm	59	58	50
Initial luminosity, 10^{30} cm^{-2}s^{-1}	40.5	35	290
Initial luminosity lifetime, hour	11	12	7.1
Store duration, hour	19	20	15.2
Luminosity integral per store, pbarn	1.71	1.2	8.65
Shot setup time, hour	2	2	2
Number of store hours per year	-	-	4800
Luminosity integral per year, fbarn	-	-	2.78
Transfer efficiency from stack to Tevatron at low-beta	60%	59%	80%
Average antiproton production rate, 10^{10}/hour	-	11	40
Total antiproton stack size, 10^{10}	166	150	610
Antiprotons extracted from the stack, 10^{10}	154	140	610

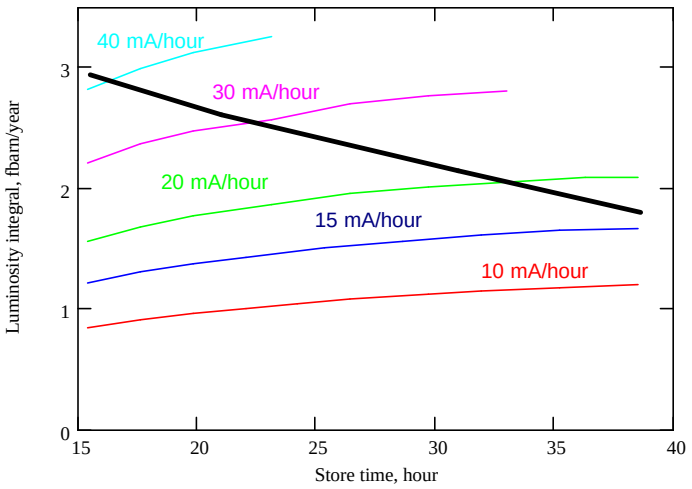

Figure 13. Dependencies of luminosity integral per year on the store time for different antiproton production rates. Thick solid line shows where intensity of antiproton beam reaches $1.35 \cdot 10^{11}$ per bunch.

Table 3. Break-up of the collider luminosity lifetime

	Lifetime [hour]
Luminosity	7.2
Prot.intens.	52
Pbar.intens.	29
Prot.H.emit.	9
Prot.V.emit.	32
Pbar.H.emit.	17
Pbar.V.emit.	56
Hourglass factor	32

6. Effects of beam-beam interaction and non-linearity of the lattice on particle diffusion

Conclusion

For correctly tuned collider at present beam intensities the beam-beam effects and machine nonlinearity, as well as, coherent effects do not produce harmful effects on the beam dynamics and collider luminosity while beams are in collisions.

References

1. V. Lebedev, S. Nagaitsev, Particle diffusion due to Coulomb scattering, EPAC 2002.
2. N.V.Mokhov, V.I.Balbekov, "Beam and luminosity lifetime", in *Handbook of Accelerator Physics and Engineering, 2-nd printing*, Ed. by A.W.Chao and M.Tigner, p.218, World Scientific (2002).
3. Lebedev V.A., et al., *NIM-A* **391**, 176-187 (1997).
4. J. D. Bjorken and S. K. Mtingwa, "Intrabeam scattering", *Particle accelerators*, (1983), v. 13, pp. 115-143.
5. The reference about spectral density of RF noise